

Study Subbarrier Fusion Reaction Dynamics in ${}^{6,7}\text{Li}$ on Light Targets by Antisymmetric Molecular Dynamics Model

D. X. Wang,¹ M. Huang,^{1,*} and S. Zhang^{1,†}

¹*College of Mathematics and Physics, Inner Mongolia Minzu University, Tongliao 028000, China.*

The subbarrier fusion reaction of ${}^{6,7}\text{Li}$ on light targets ${}^{12,13}\text{C}$, ${}^{16}\text{O}$, and ${}^{24}\text{Mg}$ using Antisymmetrized Molecular Dynamics (AMD) model were investigated. Within the AMD framework, the ground state of ${}^{6,7}\text{Li}$ is found to exhibit an $d(\alpha) + t$ configuration, and possess significant deformation. Simulations are performed in the energy range of 2 - 9 MeV center-of-mass energy (E_{cm}), proximate to the Coulomb barrier. The computed total fusion cross-sections, as a function of incident energy, is found to agree favorably with experimental data at $E_{cm} > 3$ MeV. In addition, a comparison is made between the AMD predicted cross-sections of various residue channels at $E_{cm} = 5$ MeV and corresponding experimental data.

PACS numbers: 25.70.Pq

Keywords:

I. INTRODUCTION

The availability of radioactive beam facilities has sparked considerable theoretical and experimental attention towards the examination of the breakup mechanism and structure of nuclei situated far from the stability line. These properties of the interacting nuclei play a crucial role in the context of nuclear fusion reactions near the Coulomb barrier, particularly in the presence of weakly bound neutrons [1].

The fragmentation of projectiles possessing low binding energies is known to have a significant impact on fusion reactions, resulting in distinct fusion pathways. Specifically, the process of complete fusion (CF) arises from the successful capture of the entirety of the projectile by the target. It should be noted that complete fusion (CF) may take on two distinct forms: direct CF, where the fusion occurs without prior projectile fragmentation, and sequential CF, where all projectile fragments are captured subsequent to their fragmentation. In the event that only certain fragments are captured while others evade capture, the process is deemed incomplete fusion (ICF). The summation of both complete and incomplete fusion reactions is referred to as total fusion (TF) [2].

Several theoretical computations suggest that the fusion cross-section for such nuclei may be elevated when compared to well-bound nuclei, due to the larger spatial extent of the halo nucleons [3]. Conversely, the fragility of halo nuclei, caused by their low binding energies, can result in disintegration when subjected to the field of the other nucleus prior to approaching close enough to effect fusion and release available energy. Initial calculations by Hussein *et al.* [4] suggest that the actual fusion cross-section is markedly reduced across all energies. Recent couple channel calculations of studies by Hagino *et al.* [5] have revealed that the fusion cross section exhibits a nuanced behavior in the presence of a neutron halo. Specifically, the cross section is observed to increase below the Coulomb barrier, owing to the halo's presence,

whereas it decreases above the barrier due to weak coupling of the halo nucleons. Despite these findings, experimental verification remains challenging and a topic of ongoing discussion. In addition to this, the fusion mechanism may also be influenced by the cluster structure of the participating nuclei. Theoretical investigations have explored the cluster structures of light nuclei, ranging from stable to those far from the stability line. Recent research, utilizing an antisymmetrized molecular dynamics model (AMD), has revealed the existence of various distinct cluster structures in these nuclei [6–9]. Cluster structures have been predicted for nuclei with similar numbers of protons and neutrons, such as Li and Be [7]. When such nuclei are involved in fusion reactions near the Coulomb barrier, the fusion cross section is expected to reflect the cluster structure, particularly through variations in the exit channel and fusion residue distributions. The effect of the cluster structure may be more pronounced in fusion reactions involving light systems, where the Coulomb interaction is relatively weak and the proximity effect between the nuclei is enhanced. As a result, the structure of the projectile and/or target may have a direct impact on the fusion cross section, especially by enhancing certain incomplete fusion channels.

The present study adopts the AMD/DS version [10], which due to the selection of a finite value of the coherence time, the dynamics of a system can exhibit both diffusion (D) and wave packet shrinking (S) effects, as manifested in the mean field propagation. We present the results of our investigation into the fusion reactions of the ${}^{6,7}\text{Li} + {}^{12,13}\text{C}$, ${}^{6,7}\text{Li} + {}^{16}\text{O}$, and ${}^{6,7}\text{Li} + {}^{24}\text{Mg}$ systems near the Coulomb barrier, as determined through AMD simulations.

II. AMD SIMULATIONS

The AMD/DS code, employing the Gogny interaction, was utilized to generate the initial nuclei of ${}^{6,7}\text{Li}$, ${}^{12,13}\text{C}$,

^{16}O , ^{24}Mg , and ^{28}Si . The computed binding energies and root mean square radii of these nuclei were compared with their corresponding experimental values, as summarized in Table 1. The computed values are in good agreement with the experimental data, except for the root-mean-square radius of $^{6,7}\text{Li}$, for which the computed value is approximately 20% greater than the experimental value. However, the more advanced calculation performed in reference [7] of the experimental binding energy of $^{6,7}\text{Li}$ is well reproduced, demonstrating distinct $d(\alpha) + t$ structures.

TABLE I: initial nuclei.

nucleus	AMD Binding energy (MeV)	AMD rms (fm)	Exp. Binding energy (MeV)	Exp. rms (fm)
$^6\text{Li}(d,\alpha)$	35.15	3.15	31.99	2.59
$^7\text{Li}(t,\alpha)$	40.00	3.02	39.24	2.43
^{12}C	92.24	2.53	92.16	2.47
^{13}C	104.77	2.55	97.11	2.46
^{16}O	127.51	2.67	127.62	2.70
^{24}Mg	205.13	3.24	198.24	3.06

The density plot of these nuclei are also shown in Fig.1. Symbols indicate the location of all nucleons. One can see in both figures that nucleons are well clusterized in space. The plots reveal that nucleons are tightly clustered in space. In the case of ^6Li and ^7Li , two clusters are clearly observed, with the larger one corresponding to an α and the other to a deuteron or triton, resulting in a highly deformed nucleus. Conversely, $^{12,13}\text{C}$ [11, 12], ^{16}O [13], and ^{24}Mg have no developed cluster structure and the nuclei are compact and significantly more spherical.

Using these initial nuclei, $^{6,7}\text{Li}+^{12,13}\text{C}$, $^{6,7}\text{Li}+^{16}\text{O}$, and $^{6,7}\text{Li}+^{24}\text{Mg}$ reactions were simulated at center of mass energies between 2 to 9 MeV by AMD/DS. The calculations were performed up to times ranging from 2000 fm/c and clusterized at the end of the calculation, using a coalescence technique in phase space. The coalescence radius, corresponding to 5 fm in the coordinate space, is used at all energies. The Z , A , excitation energy, angular momentum and velocity vector of each cluster were calculated. Calculations were performed in the impact parameter range, b , from 0 to 7 fm. In $b > 7$ fm, no fusion reactions are observed.

The Fig.2 depicts a comparison between the experimentally observed fusion cross sections (open circles) and those obtained through calculations filtered for proton number Z greater than the target's Z number (open squares) and filtered for Z equal to the sum of the projectiles' and targets' Z numbers (closed triangles). The experimental data was obtained from reference [15–18]. The experimental data are reproduced well within the

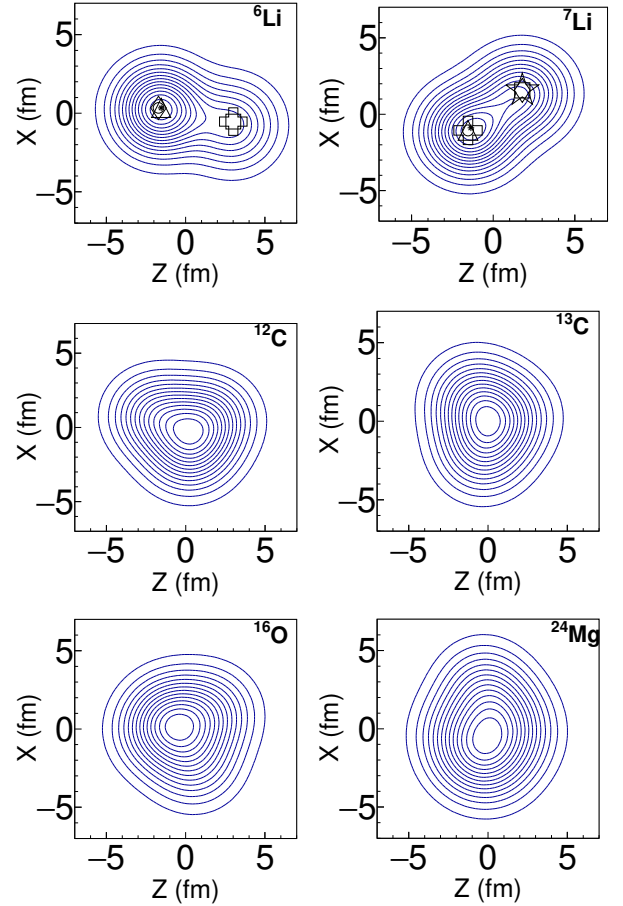


FIG. 1: Initial nucleus of $^{6,7}\text{Li}$, $^{12,13}\text{C}$, ^{16}O , and ^{24}Mg from left to right.

experimental errors above $E_{cm} > 3$ MeV in the absolute scale. The absolute cross sections predicted by the AMD simulations were calculated using the number of events generated in the given impact parameter range. At $E_{cm} \leq 3$ MeV the AMD simulation underestimated the fusion cross sections. In this energy range, the tunneling effect through the Coulomb barrier becomes important and in the present AMD formulation, this process is not incorporated. In the figure the formation cross sections of ^{19}F in the primary AMD events are also plotted by open square symbols. As discussed below, there are additional 20-30% incomplete fusion contribution in the primary fusion process.

In Fig.3 the time evolution of the density distributions is shown as typical examples of the complete and incomplete fusion reactions. On the left panel, a complete fusion reaction is observed. In the middle, only the α particle is transferred into the ^{12}C nucleus and triton is escaped as a spectator. On the right panel, only triton is absorbed and the α particle becomes a spectator. The latter two cases are mainly observed at larger impact parameters. In each incident energy, a few thousand to ten thousand events are generated, depending on the fusion

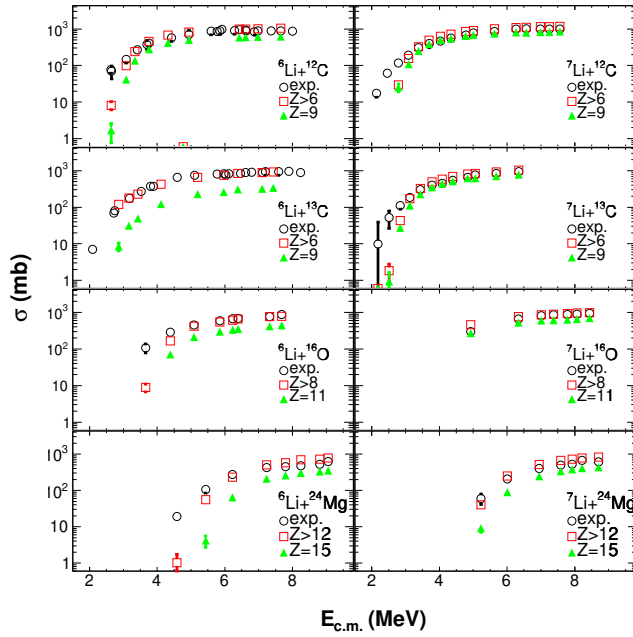


FIG. 2: Fusion cross section for the ${}^6,{}^7\text{Li} + {}^{12,13}\text{C}$, ${}^6,{}^7\text{Li} + {}^{16}\text{O}$ and ${}^6,{}^7\text{Li} + {}^{24}\text{Mg}$ systems. Circles represent experimental results and taken from [15–18]. Squares are the primary of AMD results filtered by $Z = 9, 11, 15$, respectively, whereas triangles are filtered by $Z > 6, 8, 12$ respectively.

cross section, proportional to the impact parameter in the given range.

In Fig.4, the fusion channel distribution at the primary stage is shown as a probability distribution. Only the top three major channels are plotted. The ${}^{19}\text{F}$ formation and ${}^{15}\text{N} + \alpha$ channel dominate the fusion reaction at all energies. Complete fusion occurs in about 80% of the cases at the lower incident energies and decreases to about 70% at the higher energies. The third channel contribution is from different reactions at different incident energies, but their probabilities are only a few % at most.

SUMMARY

The fusion cross section of the ${}^6,{}^7\text{Li} + {}^{12,13}\text{C}$, ${}^6,{}^7\text{Li} + {}^{16}\text{O}$ and ${}^6,{}^7\text{Li} + {}^{24}\text{Mg}$ reaction was studied using the AMD codes.

ACKNOWLEDGMENTS

We thank A. Ono for helpful discussions and communications. And thank him and R. Charity for letting us to use their calculation codes. This work was supported by the National Natural Science Foundation of China (Grants No. U2032146, 12175152, 11765014 and

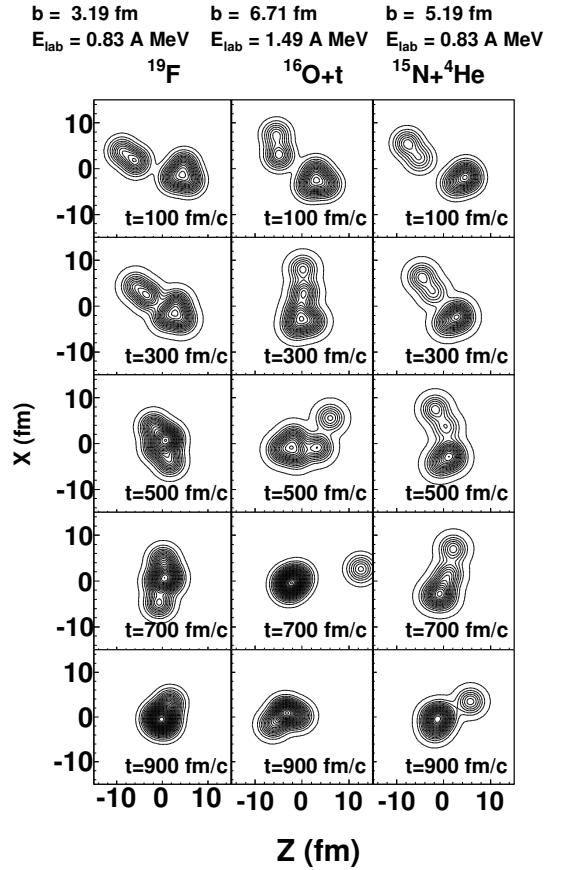


FIG. 3: Time evolution of the 2D density plots for typical fusion reactions for ${}^7\text{Li} + {}^{12}\text{C}$ system. Impact parameter, incident energy and reaction product at the bottom of the simulations are indicated on the top of each figure. The density plot is made by projecting that of all nucleons on the X-Z plane. The contour lines are plotted on a linear scale.

11609053), Natural Science Foundation of Inner Mongolia (Grants No. 2019JQ01) and the Program for Young Talents of Science and Technology in Universities of Inner Mongolia Autonomous Region (NJYT23109).

* E-mail at:huangmeirong@imun.edu.cn

† E-mail at:zsylt@imun.edu.cn

- [1] L.F. Canto *et al.*, Nucl. Phys. **A424** 1 (2006).
- [2] A. Gómez Camacho, A. Diaz-Torres, and H. Q. Zhang, Phys. Rev. **C99** 054615 (2019).
- [3] N. Takigawa *et al.*, Phys. Rev. **C47** R2470 (1993).
- [4] M.S. Hussein *et al.*, Phys. Rev. **C46**, 377 (1992); M.S. Hussein *et al.*, Phys. Rev. Lett. **72**, 2693 (1994); M.S. Hussein *et al.*, Nucl. Phys. **A588**, 85c (1995).
- [5] K. Hagino *et al.*, Phys. Rev. **C61** 037602 (2000).
- [6] Y. Kaneda-En'yo *et al.*, Phys. Rev. **C52**, 628 (1995)
- [7] Y. Kaneda-En'yo *et al.*, Phys. Rev. **C52**, 647 (1995)
- [8] Y. Kanada-En'yo *et al.*, Phys. Rev. **C60**, 064304 (1999);

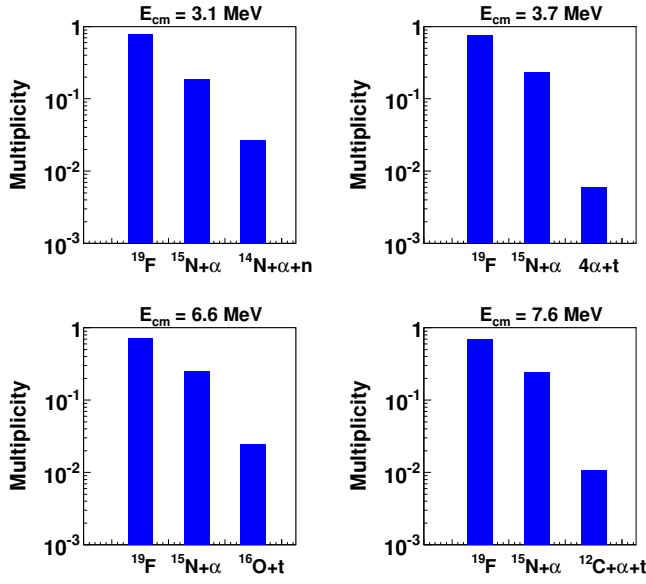


FIG. 4: Primary major exit channel distribution at different incident energies for ${}^7\text{Li} + {}^{12}\text{C}$ system.

- [9] Naoya Furutachi, Masaaki Kimura, Akinobu Doté and Yoshiko Kanada-En'yo, Prog. Theor. Phys. **122**, 865 (2009).
- [10] A. Ono, H. Horiuchi, Prog. Part. Nucl. Phys. **53**, 501 (2004).
- [11] Yoshiko Kanada-En'yo, Prog. Theor. Phys. **117**, 655 (2007).
- [12] Y. Chiba and M. Kimura, Phys. Rev. **C101**, 024317 (2020).
- [13] Yoshiko Kanada-En'yo, Phys. Rev. **C96**, 034306 (2017).Erratum Phys. Rev. **C101**, 069901 (2020).
- [14] R. J. Charity *et al.*, Nucl. Phys. **A483**, 371, 1988.
- [15] A. Mukherjee *et al.*, Nucl. Phys. **A596**, 299 (1996).
- [16] A. Mukherjee *et al.*, Nucl. Phys. **A635**, 305 (1998).
- [17] A. Mukherjee *et al.*, Nucl. Phys. **A645**, 13 (1999).
- [18] M. Ray *et al.*, Phys. Rev. **C78**, 064617 (2008).